J Appl Electrochem (2014) 44:309–316
DOI 10.1007/s10800-013-0636-0

RESEARCH ARTICLE

KOH-activated depleted fullerene soot for electrochemical double-layer capacitors

Li Sun · Chunlei Wang · Ying Zhou · Xu Zhang · Jieshan Qiu

Received: 17 July 2013 / Accepted: 7 October 2013 / Published online: 18 October 2013

Abstract Nanostructured activated carbons for electrochemical double-layer capacitors were synthesized from depleted fullerene soot (DFS) via KOH activation. The structural and textural properties of the activated DFS were studied using transmission electron microscopy, X-ray diffraction, and nitrogen sorption. Activated DFS with high specific surface areas (SSAs) of up to 2,153 $m^2\ g^{-1}$ and narrow pore size distributions (PSDs) was obtained by controlling the KOH/DFS ratio. The activated DFS exhibited excellent capacitive behavior, with a high specific capacitance of 250 $F\ g^{-1}$ at a current density of 50 $mA\ g^{-1}$ in a 6 M KOH electrolyte, and a high rate performance, with a capacitance retention of up to 80 % at a high scan rate of 200 $mV\ s^{-1}$. Moreover, the activated DFS samples exhibited good electrochemical stability; high capacitance retention ratios of >90 % were obtained at a current density of 2,000 $mA\ g^{-1}$ for 5,000 cycles with cell voltages of 0.9 and 1.0 V in a two-electrode system. The high electrochemical performance can be attributed to high SSAs, narrow PSDs, and nanoscale particle sizes, which facilitate the formation of electrochemical double layers and rapid ion diffusion.

Keywords Depleted fullerene soot · Activated carbon · Activation · Electrochemical double-layer capacitor

L. Sun · C. Wang · Y. Zhou (✉) · X. Zhang · J. Qiu (✉)
Carbon Research Laboratory, Liaoning Key Lab for Energy Materials and Chemical Engineering, State Key Lab of Fine Chemicals, School of Chemical Engineering, Dalian University of Technology, Dalian 116024, China
e-mail: zhouying.dlut@dlut.edu.cn

J. Qiu
e-mail: jqiu@dlut.edu.cn

1 Introduction

There is increasing interest in using carbon nanomaterials (e.g., graphene, carbon nanotubes, carbon nanofibers, and carbon onions) in electrochemical double-layer capacitors (EDLCs) due to their unique structures, high conductivity, good corrosion resistance, and high stability [1–3]. It is well known that the performance of carbon materials as EDLCs is strongly dependent on factors such as the specific surface area (SSA), pore size distribution (PSD), particle size, electrical conductivity, and surface chemistry. Among these factors, the SSA plays an essential role in the EDLCs, according to the charge storage mechanism [1]. However, the majority of nanocarbons have lower SSAs than porous carbons. Therefore, the specific capacitances of most nanoscale polymorphs of carbon are significantly lower than those of commercial activated carbons. To improve the performance of nanocarbons, a chemical activation process, especially using KOH as an activating agent, is often adopted because carbon materials with exceptionally high SSAs can easily be obtained in this manner [4]. The KOH activation of multi-walled carbon nanotubes (MWCNTs) was developed by Frackowiak et al. [5]. The SSA of MWCNTs increases at least fourfold (up to 885 $m^2\ g^{-1}$) after the activation process, and the capacitance value increases from 15 to 90 $F\ g^{-1}$ in alkaline media. Activated carbon nanofibers exhibit a SSA increase from 13 to 212 $m^2\ g^{-1}$ following KOH activation, and a moderate capacitance of 60 $F\ g^{-1}$ is obtained due to the low SSA [6]. However, KOH-activated amorphous carbon nanofibers present a high SSA of up to 1,520 $m^2\ g^{-1}$ and a capacitance of 200 $F\ g^{-1}$ [7]. Porous carbon materials with BET surface areas of up to 3,100 $m^2\ g^{-1}$ were recently synthesized by Zhu et al. [8] through the KOH activation of two-dimensional nanocarbon, i.e., exfoliated graphene

oxide. The graphene-based nanostructured carbon materials exhibit high specific capacitance and energy density values.

Depleted fullerene soot (DFS) is the insoluble residue obtained after the extraction of fullerenes from the soot that is produced by laser ablation, arc-discharge, or flames [9–11]. Improved technology has led to highly feasible process for the mass production of fullerenes, which can be produced with a capacity of more than tens of tons per year, especially using the flame-based method [12]. DFS constitutes ca. 90 % of the original soot; however, determining how to reuse these materials remains a problem. Chen et al. [13] and Cleveland et al. [14] investigated the use of DFS as a carbonaceous adsorbent. Our group has recently synthesized high-quality double-walled carbon nanotubes from DFS using the arc-discharge method [15]. Silva et al. [16] investigated the surface and electrochemical properties of DFS using the thin porous coating electrode technique and found that heat-treated DFS has a higher charge storage capacity than Vulcan XC-72 carbon powder. In contrast to other porous carbon materials, DFS is composed of nanosized particles with amorphous and fullerenic carbons (curved graphitic layers and closed-shell structures) [17]. Such a positive curvature and the nanoscale particle size of DFS facilitate the accessibility of counter-ions; therefore, the rapid charge/discharge properties of the DFS should be expected for EDLC materials [18, 19]. In fact, the specific capacitance of DFS is only 58 F g^{-1} due to the low SSA of 491 m^2 g^{-1} [20]. The low SSA of DFS limits their energy storage applications. Thus, the main objective of this work is to prepare porous nanocarbons with high SSAs from DFS by KOH activation and to further explore their application as electrode materials for EDLCs.

2 Experimental

2.1 Sample preparation

DFS produced from benzene flames was kindly provided by the JingMeng Hi-Tech Corp. Chemical activation with KOH was conducted as follows: 1 g of DFS was soaked in a solution that contained 10 ml of water and 2, 4, 6, or 8 g of KOH at room temperature. The resulting slurry was dried overnight at 383 K before activation. The activation was performed in a horizontal furnace, and the samples were heated (5 K min^{-1}) from room temperature to the final temperature (973/1,073/1,173 K) for 1 h under a nitrogen atmosphere. The activated samples were washed with 1 M HCl and then washed with distilled water until a neutral pH was achieved. Then, the samples were dried at 383 K for 12 h. The products were designated as DFS-x-y, where x is the ratio of KOH/DFS and y is the activation temperature in K. Non-activated carbon was also prepared at 1,073 K for 1 h as a reference material, and it was designated DFS-0-1073.

2.2 Sample characterization

Nitrogen sorption measurements were performed at 77 K using a Quantachrome Autosorb-1-MP adsorption instrument. Prior to the measurements, the samples were degassed at 473 K for 4 h. The SSAs (S_{BET}) were calculated using the Brunauer–Emmett–Teller equation over a relative pressure range of 0.06–0.35. The micropore volumes (V_{mic}) and the micropore surface areas (S_{mic}) were determined using the t-plot method, and the total pore volumes (V_T) were determined at a P/P_0 of 0.95. The volumes of mesopores (V_{mes}) were obtained from V_T–V_{mic}. The PSDs of the samples were obtained using the density functional theory (DFT) approach. X-ray diffraction (XRD, 40 kV, 100 mA) patterns were collected on a Rigaku D/Max2400 diffractometer equipped with a Cu-Kα radiation source. The as-obtained DFS and activated DFS samples were also examined using transmission electron microscopy (TEM, Philips Tecnai G^2 F30).

2.3 Electrochemical measurements

The capacitor electrodes were obtained by pressing a mixture of the activated DFS (80 wt%), carbon black (10 wt%), and polytetrafluoroethylene (10 wt%) into nickel foam collectors. The diameter of the electrodes was 10 mm. The cyclic voltammetry (CV) tests were conducted using an electrochemical working station (CHI660D, Shanghai, China) in a three-electrode cell, employing a platinum foil as the counter electrode and Hg/HgO as the reference electrode. CVs were recorded between −0.9 and −0.1 V at different scan rates. Specific capacitances were derived from the CV curves using the equation $C = (\int i dV)/(2\upsilon m V)$, where C (F g^{-1}), i (A), m (g), υ (V s^{-1}), and V (V) are the specific capacitance, the instant current on the CV curves, the mass of active electrode material, the potential scan rate, and the potential of the CV tests, respectively. The galvanostatic charge/discharge (GC) measurements were conducted on a battery testing system (Land CT 2001, Wuhan, China) over the potential range of −0.9 to −0.1 V. The specific capacitances (C_g, F g^{-1}) of the DFS electrodes were calculated from the discharge curves under different loading current densities according to the equation $C_g = I\Delta t/m\Delta V$, where I (A) is the discharge current, Δt (s) is the discharge time, m (g) is the mass of the active carbon material of the working electrode, and ΔV (V) is the potential difference during discharge. If a two-electrode system was used, two capacitor electrodes with identical sizes and masses were mounted face-to-face

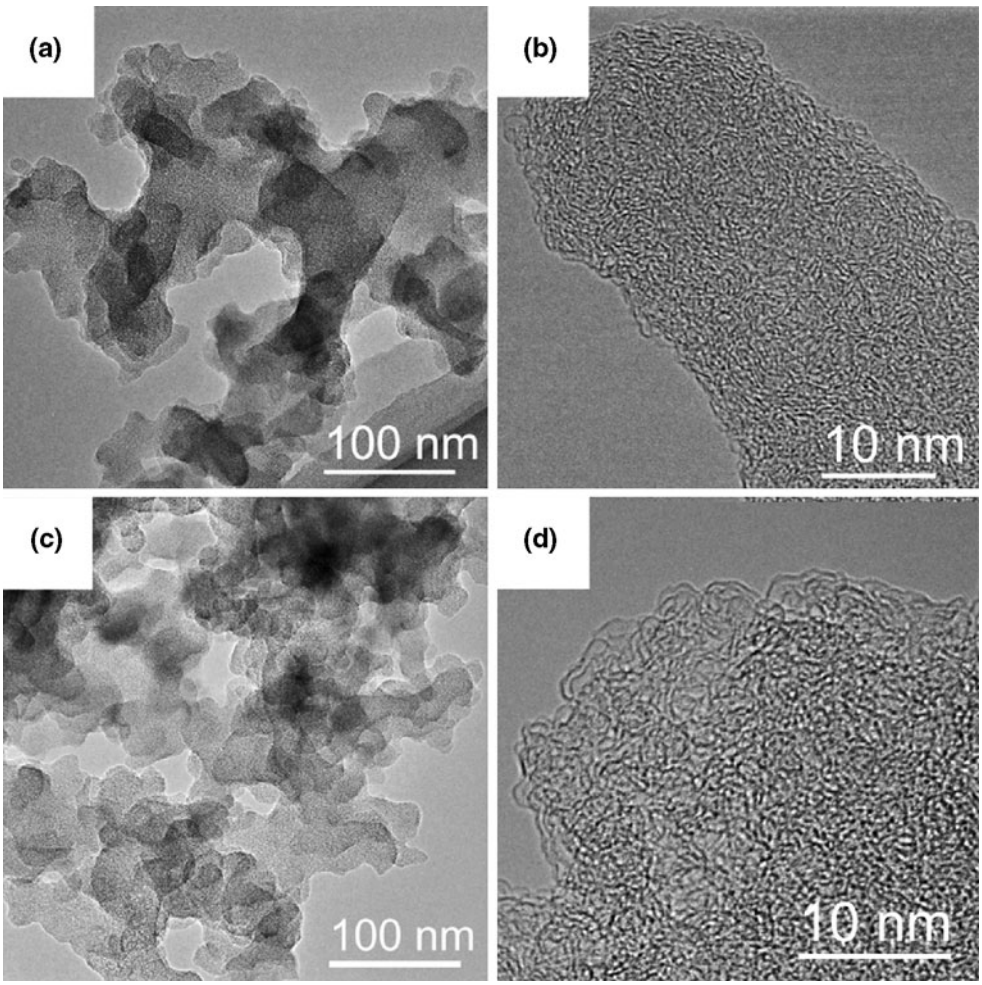

Fig. 1 TEM images and high-resolution TEM images of **a**, **b** DFS and **c**, **d** DFS-4-1073, respectively

in the Teflon cell holder and separated by a non-woven separator. The specific capacitance ($C_{g,\ cell}$, F g^{-1}) was calculated from the discharge curves according to $C_{g,\ cell} = 2I\Delta t/m\Delta V$, where I (A) is the discharge current, Δt (s) is the discharge time, m (g) is the mass of the active carbon material of the single electrode, and ΔV (V) is the potential window (0.9 or 1.0 V). All the electrochemical experiments were performed in a 6 M KOH aqueous solution at room temperature. The electrolytes were degassed with nitrogen for 2 h before use.

3 Results and discussion

3.1 TEM and XRD analysis

Typical TEM images of the DFS before and after KOH activation are shown in Fig. 1. The TEM observation of the as-obtained DFS reveals that it is a typical 3-dimensional fractal nanostructure [17, 21]. After KOH activation, the morphologies of DFS-4-1073 retain their hierarchical nanostructures. Other than disordered planar carbon sheets, which are known to be carbon black, the high-resolution TEM image of DFS suggests that the soot is composed of stacks of bent carbon layer fragments with ragged edges formed by globular and semi-closed carbon nanocapsules, as shown in Fig. 1b [17]. Loosely arranged curved carbon sheets can be observed in the high-resolution TEM image of DFS-4-1073 (Fig. 1d), indicating that pores were effectively generated by the KOH etching process. Irregular carbon capsules with uniform shell thicknesses and nanosized cavities are observed at the edges of the activated samples. The curvature of the carbon sheets in the DFS is considered to be due to the incorporation of pentagons or heptagons in the carbon network; thus defects can be preserved in the activated samples.

XRD patterns of the samples before and after activation are shown in Fig. 2. A sharp peak at $2\theta = 26°$, which can be assigned to the (002) panel of a lamellar benzenoid lattice (molecular aromatic solid or graphite sheet), is

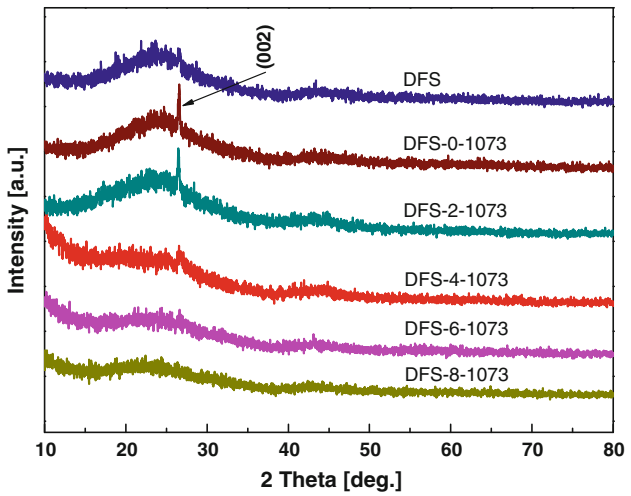

Fig. 2 XRD patterns of the samples

observed after thermal treatment at 1,073 K, suggesting the transformation of polymerization polycyclic aromatic hydrocarbons and/or metastable fullerenic structures to more stable lamellar crystallites [22]. It is well known that the extremely high SSAs of carbon materials activated with KOH are attributed to partial gasification and expansion of the graphene layers through simultaneous intercalation and deintercalation of metallic potassium. In addition, slit-shaped micropores are believed to originate from the expansion of graphene layers during the rapid removal of the intercalated potassium [23]. The intensity of the (002) diffraction peak decreases as the KOH/DFS ratio increases from 2/1 to 6/1, and this peak nearly disappears as the KOH/DFS ratio increases to 8/1 (see Fig. 2), indicating that the graphitic layers expand during the development of micropores.

3.2 Nitrogen sorption

Although there have been several works on improving the SSA of DFS through either heat treatments or CO_2 activation, only carbon materials with moderate SSAs (500–700 $m^2\ g^{-1}$) have been obtained [24, 25]. Thus, DFS with a high SSA is highly desirable for EDLC applications. In this work, the mass ratio of KOH/DFS and the activation temperature are confirmed to be key parameters for the development of a high SSA and a narrow PSD. Figure 3a presents the nitrogen sorption isotherms of DFS samples activated at 1,073 K with different KOH/DFS ratios. Abrupt increases in the adsorption of all activated samples at low relative pressures are observed, which is characteristic of micropores (<2 nm). The samples with KOH/DFS ratios of less than 4/1 yield represent type I isotherms. An obvious step associated with the filling of mesopores due to the capillary condensation of nitrogen occurs at the

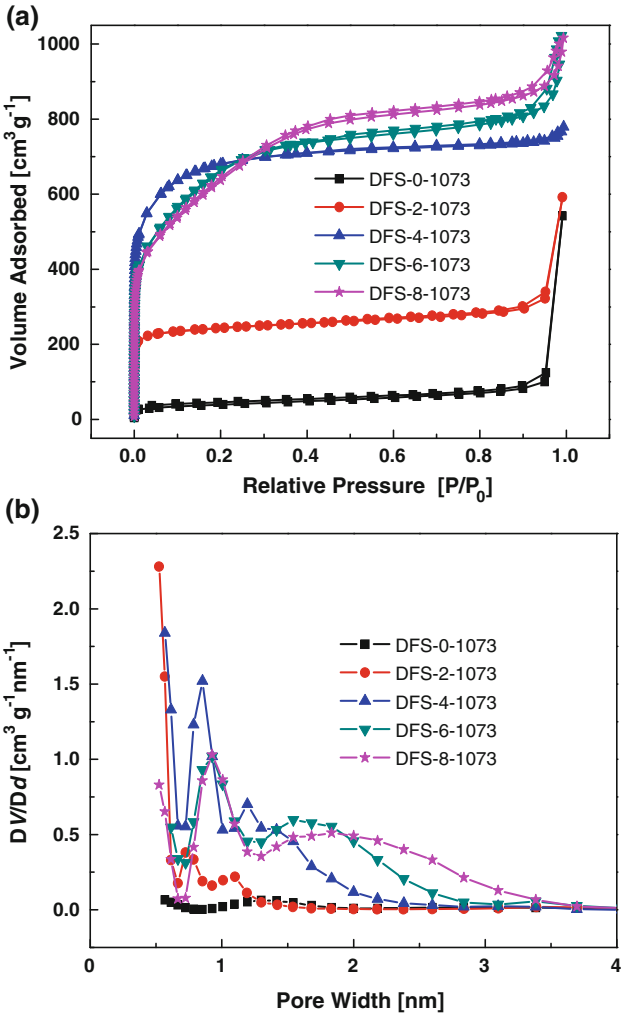

Fig. 3 **a** Nitrogen sorption isotherms and **b** DFT PSDs of the samples

media relative pressure when increasing the KOH/DFS ratio to 6/1. Moreover, mesopores are also observed to be easily developed by increasing the activation temperature to 1,173 K with the KOH/DFS ratio of 4/1 (Table 1). This result indicates that the development of micropores occurred predominantly below 1,073 K, whereas the development of mesopores is favored at high temperatures [26]. The textural properties and specific capacitances of all samples are summarized in Table 1. Before activation, the DFS-0-1073 sample exhibits only a small pore volume (0.17 $cm^3\ g^{-1}$) and a low SSA (130 $m^2\ g^{-1}$). The pore volumes and SSAs of the activated DFS increase as the KOH/DFS ratio increases. Sharp increases in the SSA (from 701 to 1,989 $m^2\ g^{-1}$) and pore volume (from 0.50 to 1.15 $cm^3\ g^{-1}$) are observed as the KOH/DFS ratio increases from 2/1 to 4/1, and slight increases are obtained when the KOH/DFS ratio is greater than 4/1. Figure 3b shows the DFT PSDs of DFS-x-1073. The porosities of DFS-x-1073 are mainly micropores (<2 nm) and that the

Table 1 Structural parameters of the samples

Sample	S_{BET} (m^2 g^{-1})	S_{mic} (m^2 g^{-1})	V_T (cm^3 g^{-1})	V_{mic} (cm^3 g^{-1})	V_{mes} (cm^3 g^{-1})
DFS-0-1073	130	30	0.17	0.04	0.13
DFS-2-1073	701	568	0.50	0.35	0.15
DFS-4-1073	1989	1,727	1.15	0.95	0.20
DFS-6-1073	2,063	1,438	1.29	0.77	0.52
DFS-8-1073	2,153	943	1.37	0.49	0.88
DFS-4-973	1,237	1,015	0.77	0.56	0.21
DFS-4-1173	1,767	988	1.14	0.53	0.61

PSDs gradually become wide, indicating that the excess amount of KOH etches and enlarges the existing micropores as the KOH ratio increases. Compared with activated carbons derived from other nanotextured carbons, such as carbon nanotubes and carbon nanofibers, the activated DFS possesses not only a high SSA but also a narrow PSD [5, 27]. For activated graphene, the SSA is as high as 3,100 m^2 g^{-1}, but the PSD is much broader, in the range of 0.5–10 nm [8]. Furthermore, the high cost of graphene also limits its application.

3.3 Electrochemical characterization of samples

CV and GC techniques were used to characterize the capacitive properties of the samples. All the activated samples exhibit typical capacitive behavior with a rectangular-like CV curve shape, indicating that the capacitive response primarily comes from the electrochemical double-layer mechanism (Fig. 4a, b). The areas surrounded by the CV curves of DFS-4-973 and DFS-4-1073 are slightly larger than that of DFS-4-1173 (Fig. 4a), which is consistent with the nitrogen sorption results. Furthermore, a better rectangular-like CV curve shape is also found when increasing the activation temperature to 1,073 K. Figure 4b presents the CV curves of samples with different KOH/DFS ratios when the activation temperature is fixed at 1,073 K. Before activation, the CV curve of DFS-0-1073 yields a small area due to a low SSA (130 m^2 g^{-1}) and low micropore volume (0.04 cm^3 g^{-1}). The CV curve areas of the activated samples were clearly enlarged, corresponding to the increase in the surface area and micropore volume (Table 1).

The effect of the sweep rate on the CV curves of DFS-x-1073 was investigated. Typical CV curves for DFS-4-1073 (Fig. 5a) at different potential scan rates exhibit excellent electrochemical behavior over a wide scan rate range of 10–300 mV s^{-1}. As the scan rates increase (even up to 300 mV s^{-1}), only minimal distortions of the rectangular-shaped CV curves are observed, implying that the activated DFS-4-1073 samples have a larger surface area that is accessible to ion adsorption and a quicker electrolyte ion diffusion rate compare with the non-activated sample (DFS-0-1073), which exhibits only small and distorted rectangular curves (Fig. 5b). Figure 5c and d show the relationships of the specific capacitance and the capacitance retention ratio of the samples as a function of the potential scan rates with different KOH/DFS ratios and a fixed activation temperature of 1,073 K, respectively. The capacitance value of DFS is significantly enhanced after activation due to the rapid increase in SSA (the specific capacitance of pristine or thermally treated DFS is less than 70 F g^{-1}) and micropore volumes [16, 20]. The specific capacitance value increases rapidly as the KOH/DFS ratio increases from 2/1 to 4/1, and the highest capacitance is achieved with a KOH/DFS ratio of 4/1. The activated DFS also demonstrate excellent capacitance retention ratios of greater than 80 % at a high scan rate of 200 mV s^{-1} when the KOH/DFS ratio increases to ≥4/1 (Fig. 5d).

It has recently been reported that micropores (with diameters of 0.7–2 nm) play an essential role for the formation of double-layer capacitance, and mesopores are more favorable than micropores for ion diffusion [28, 29]. The PSDs of the activated DFS are primarily micropores in the range of 0.7–2 nm, and additional mesopores can be generated because of the extensive etching of the preformed micropores by the excess amount of KOH (Table 1). Figure 6a presents the specific capacitance values versus S_{mic} for the activated DFS. It is observed that the capacitance values

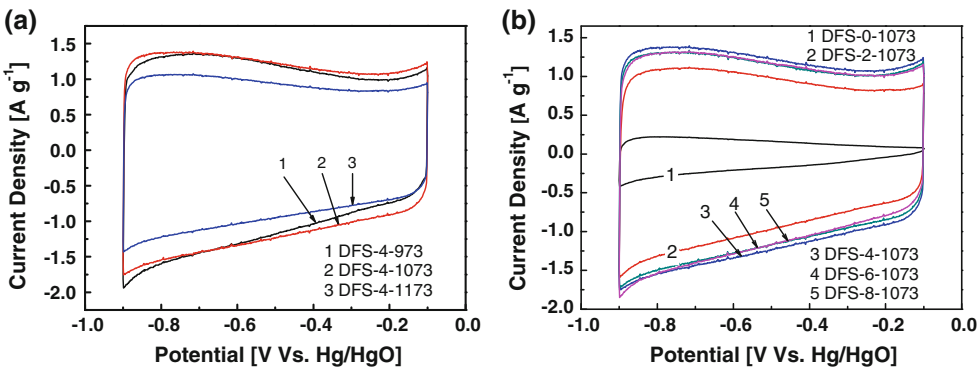

Fig. 4 CV curves of the samples with **a** the different activation temperatures and **b** different KOH/DFS ratios at a scan rate of 5 mV s^{-1}

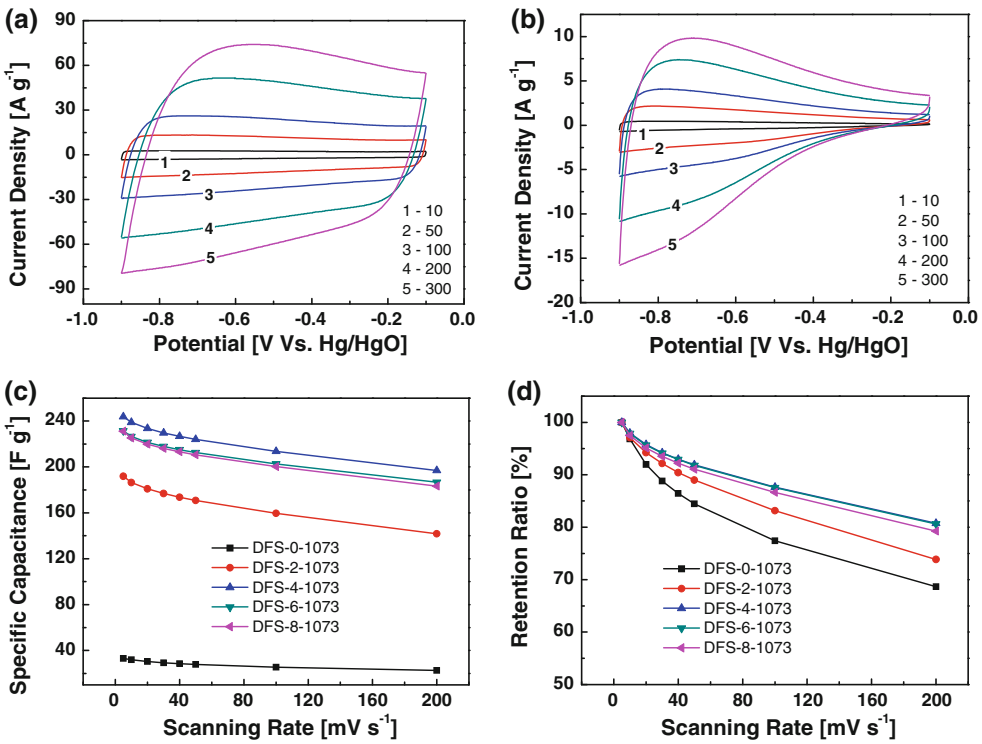

Fig. 5 CV curves of **a** DFS-4-1073 and **b** DFS-0-1073 at different scan rates; **c** the specific capacitance and **d** the capacitance retention ratios of the samples at different potential scan rates

show good correlation with the increase of the S_{mic}. The maximum S_{mic} is achieved using the KOH/DFS ratio of 4, and the highest specific capacitance was then achieved. In Fig. 6b, the capacitance retention ratio is plotted against the ratio of mesopore volume to total pore volume, V_{mes}/V_{tol}. For conventional activated carbons using bulk phase precursors (e.g., coal, coke, and carbon fiber) often possess the long and devious pores, the higher the mesopore content, the higher capacitance retention ratio should be expected at a high scan rate or current density because the mesopores act as channels or reservoirs for electrolyte transport [30, 31]. However, in this study, the V_{mes}/V_{tol} ratio has little influence on the capacitance retention ratio for the activated DFS, which can be ascribed to the following reasons. On one hand, according to previous studies, zero-dimensional or one-dimensional nanocarbons (e.g., carbon onions and carbon nanotubes) with positive graphitic curvatures demonstrate excellent rate performance due to their readily accessible external surface to ions [18, 32, 33]. The DFS used in this study is composed of nanosized fullerenic particles with curved layers and closed-shell structures according to structure characterization, which should be favorable for the adsorption/desorption of ions [17, 18]. Such positive curvature morphologies persisted very well after KOH activation, and micropores with negative curvature were subsequently generated [5, 27]. On the other hand, compared with the long and devious pores of conventional activated carbons, the inner pores of the activated DFS are much shorter due to the small particle size, which is beneficial for rapid ion transport also [1, 31, 34]. In addition, for common bulk phase precursors, the high V_{mes}/V_{tol} ratio often related with the high KOH amount and the low carbon yield, which will lead to severe corrosion of the equipment and high cost of the product. Therefore, from the economy and the eco-friendly point of view, nanostructured-activated DFS is a promising candidate for EDLC electrode materials with high rate performance.

The rate performance of DFS-4-1073 was also tested by GC at various current densities (Fig. 7a). It is clear that the DFS has typical triangular-shaped curves, indicating good capacitive behaviors even at a high current loading of 4,000 mA g^{-1}. Figure 7b presents the relationship between the specific capacitance and the charge/discharge current density. The specific capacitances slightly decrease as the current density increases (Fig. 7b), and the activated samples maintained >90 % of their capacities. In general, the ability for charges to accumulate in the interface of the electrode and electrolyte is greater with higher SSA carbons [1]. The non-activated DFS-0-1073 sample exhibits a low specific capacitance of only 55 F g^{-1}, which correlates with its low SSA (130 m^2 g^{-1}). Significant enhancements (at least fourfold) in capacitive performance are observed after KOH activation. The DFS-4-1073 sample exhibits a high capacitive performance of up to 250 F g^{-1} and a capacitance retention ratio of greater than 90 % at a high current density of 4,000 mA g^{-1}.

In addition, the capacitive durability performance of DFS-4-1073 (as shown in Fig. 8) was investigated using GC measurements in a two-electrode system at a current

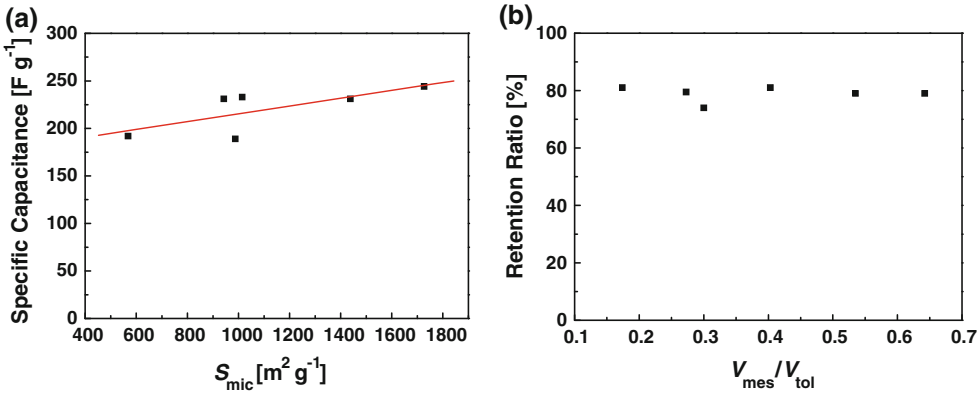

Fig. 6 **a** Specific capacitance versus S_{mic} for the activated DFS at a scan rate of 5 mV s^{-1}; **b** the capacitance retention ratio versus V_{mes}/V_{tol} for the activated DFS at a scan rate of 200 mV s^{-1}

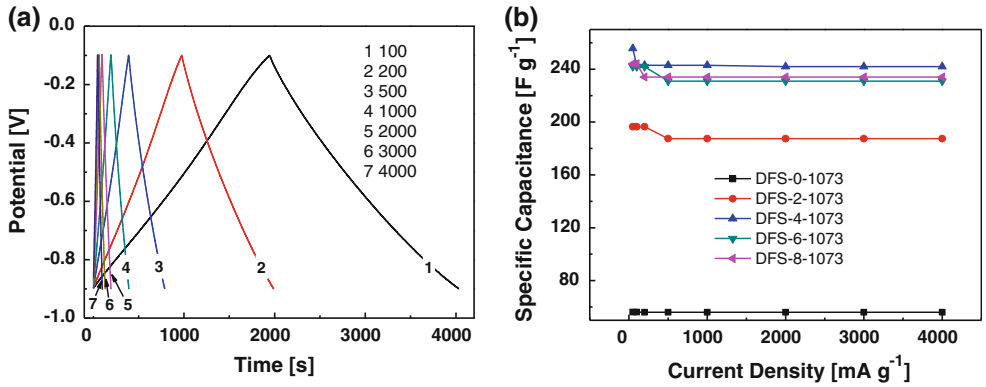

Fig. 7 **a** GC profiles of DFS-4-1073 at different current densities from 100 to 4,000 mA g^{-1}, and **b** specific capacitance of DFS-x-1073 at different current densities from 50 to 4,000 mA g^{-1}

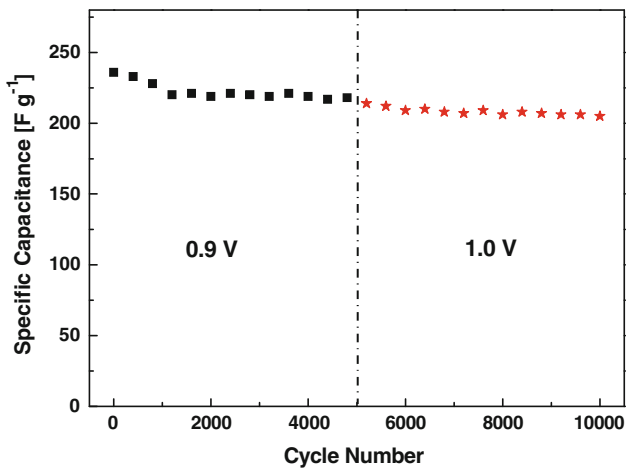

Fig. 8 Cycling performance of DFS-4-1073 at a current density of 2,000 mA g^{-1} and cell voltages of 0.9 and 1.0 V

density of 2,000 mA g^{-1}. DFS-4-1073 exhibits good capacitance retentions of greater than 90 % after 5,000 cycles at a voltage of 0.9 V and of 95 % after 5,000 cycles at 1.0 V. The excellent electrochemical stability could be attributed to the easily accessible positive curvature surface for the adsorption of ions and the short distance for their transport.

4 Conclusions

Nanostructured activated carbons were synthesized via a KOH activation process using DFS as a precursor. The SSA and the porosity of the DFS were significantly enhanced after activation, and the PSDs can be easily tailored through the KOH/DFS ratios. The activated DFS exhibits improved electrochemical properties, with a specific capacitance of up to 250 F g^{-1}, an excellent rate performance and good cycling stability, with capacitance retention ratios of greater than 90 % after 5,000 cycles. The high specific capacitances are attributed to the large SSAs and high micropore volumes, which facilitate the formation of an electrochemical double-layer. The excellent rate performances can be attributed to optimized PSDs, short inner pores, and the nanostructured morphologies with a unique positive curvature structure, which enhances the diffusion rate of ions. The present work not only provides an alternative route for the large-scale and low-cost synthesis of high-performance EDLC electrode materials but also provides a cost-effective approach for the utilization of DFS.

Acknowledgments This work was supported by the National Natural Science Foundation of China (Nos. 20836002, 21003016,

21276045), the Dalian Science and Technology Bureau of China (No. 2011A15GX023), and China Postdoctoral Science Foundation (No. 20100481227).

References

1. Frackowiak E, Béguin F (2001) Carbon materials for the electrochemical storage of energy in capacitors. Carbon 39:937–950. doi:10.1016/s0008-6223(00)00183-4
2. Pandolfo AG, Hollenkamp AF (2006) Carbon properties and their role in supercapacitors. J Power Sources 157:11–27. doi:10.1016/j.jpowsour.2006.02.065
3. Zhang LL, Zhou R, Zhao XS (2010) Graphene-based materials as supercapacitor electrodes. J Mater Chem 20:5983–5992. doi:10.1039/C000417K
4. Wang J, Kaskel S (2012) KOH activation of carbon-based materials for energy storage. J Mater Chem 22:23710–23725. doi:10.1039/C2JM34066F
5. Frackowiak E, Delpeux S, Jurewicz K, Szostak K, Cazorla-Amoros D, Béguin F (2002) Enhanced capacitance of carbon nanotubes through chemical activation. Chem Phys Lett 361:35–41. doi:10.1016/S0009-2614(02)00684-X
6. Merino C, Soto P, Vilaplana-Ortego E, de Salazar JMG, Pico F, Rojo JM (2005) Carbon nanofibres and activated carbon nanofibres as electrodes in supercapacitors. Carbon 43:551–557. doi:10.1016/j.carbon.2004.10.018
7. Barranco V, Lillo-Rodenas MA, Linares-Solano A, Oya A, Pico F, Ibañez J, Agullo-Rueda F, Amarilla JM, Rojo JM (2010) Amorphous carbon nanofibers and their activated carbon nanofibers as supercapacitor electrodes. J Phys Chem C 114:10302–10307. doi:10.1021/jp1021278
8. Zhu YW, Murali S, Stoller MD, Ganesh KJ, Cai WW, Ferreira PJ, Pirkle A, Wallace RM, Cychosz KA, Thommes M, Su D, Stach EA, Ruoff RS (2011) Carbon-based supercapacitors produced by activation of graphene. Science 332:1537–1541. doi:10.1126/science.1200770
9. Kroto HW, Heath JR, O'Brien SC, Curl RF, Smalley RE (1985) C_{60}: buckminsterfullerene. Nature 318:162–163. doi:10.1038/318162a0
10. Howard JB, McKinnon JT, Johnson ME, Makarovsky Y, Lafleur AL (1992) Production of C_{60} and C_{70} fullerenes in benzene-oxygen flames. J Phys Chem 96:6657–6662. doi:10.1021/j100195a026
11. Krätschmer W, Lamb LD, Fostiropoulos K, Huffman DR (1990) Solid C_{60}: a new form of carbon. Nature 347:354–358. doi:10.1038/347354a0
12. Murayama H, Tomonoh S, Alford JM, Karpuk ME (2004) Fullerene production in tons and more: from science to industry. Fuller Nanotub Carbon Nanostruct 12:1–9. doi:10.1081/FST-120027125
13. Chen C, Chen J, Wang X, Liu S, Sheng G, Fu J (2000) Fullerenes-extracted soot: a new adsorbent for collecting volatile organic compounds in ambient air. J Chromatogr A 886:313–317. doi:S0021-9673(00)00450-7
14. Cleveland TG, Garg S, Rixey WG (1996) Feasibility of fullerene waste as carbonaceous adsorbent. J Environ Eng ASCE 122:235–238. doi:10.1061/(ASCE)0733-9372(1996)122:3(235)
15. Qiu JS, Chen G, Li ZT, Zhao ZB (2010) Preparation of double-walled carbon nanotubes from fullerene waste soot by arc-discharge. Carbon 48:1312–1315. doi:10.1016/j.carbon.2009.01.036
16. Silva SAM, Perez J, Torresi RM, Luengo CA, Ticianelli EA (1999) Surface and electrochemical investigations of a fullerene soot. Electrochim Acta 44:3565–3574. doi:10.1016/S0013-4686(99)00111-5
17. Grieco WJ, Howard JB, Rainey LC, Vander Sande JB (2000) Fullerenic carbon in combustion-generated soot. Carbon 38:597–614. doi:10.1016/S0008-6223(99)00149-9
18. Huang JS, Sumpter BG, Meunier V, Yushin G, Portet C, Gogotsi Y (2010) Curvature effects in carbon nanomaterials: exohedral versus endohedral supercapacitors. J Mater Res 25:1525–1531. doi:10.1557/Jmr.2010.0195
19. Portet C, Yushin G, Gogotsi Y (2008) Effect of carbon particle size on electrochemical performance of EDLC. J Electrochem Soc 155:A531–A536. doi:10.1149/1.2918304
20. Egashira M, Okada S, Korai Y, Yamaki J-I, Mochida I (2005) Toluene-insoluble fraction of fullerene-soot as the electrode of a double-layer capacitor. J Power Sources 148:116–120. doi:10.1016/j.jpowsour.2005.02.003
21. di Stasio S (2001) Electron microscopy evidence of aggregation under three different size scales for soot nanoparticles in flame. Carbon 39:109–118. doi:10.1016/S0008-6223(00)00099-3
22. Kanowski M, Vieth HM, Lüders K, Buntkowsky G, Belz T, Werner H, Wohlers M, Schlögl R (1997) The structure of fullerene black and the incorporation of C_{60} investigated by ^{13}C NMR. Carbon 35:685–695. doi:10.1016/S0008-6223(97)00015-8
23. Xue R, Shen Z (2003) Formation of graphite-potassium intercalation compounds during activation of MCMB with KOH. Carbon 41:1862–1864. doi:10.1016/S0008-6223(03)00161-1
24. Egashira M, Araki T, Korai Y, Mochida I (1999) Some properties of carbon disks prepared from the toluene insoluble fraction in fullerene soot. Carbon 37:27–31. doi:10.1016/s0008-6223(98)00183-3
25. Harris PJF, Tsang SC, Claridge JB, Green MLH (1994) High-resolution electron-microscopy studies of a microporous carbon produced by arc-evaporation. J Chem Soc Faraday Trans 90:2799–2802. doi:10.1039/FT9949002799
26. Zeng XH, Wu DC, Fu RW, Lai HJ, Fu JJ (2008) Preparation and electrochemical properties of pitch-based activated carbon aerogels. Electrochim Acta 53:5711–5715. doi:10.1016/j.electacta.2008.03.035
27. Yoon SH, Lim S, Song Y, Ota Y, Qiao W, Tanaka A, Mochida I (2004) KOH activation of carbon nanofibers. Carbon 42:1723–1729. doi:10.1016/j.carbon.2004.03.006
28. Zhai Y, Dou Y, Zhao D, Fulvio PF, Mayes RT, Dai S (2011) Carbon materials for chemical capacitive energy storage. Adv Mater 23:4828–4850. doi:10.1002/adma.201100984
29. Raymundo-Piñero E, Kierzek K, Machnikowski J, Béguin F (2006) Relationship between the nanoporous texture of activated carbons and their capacitance properties in different electrolytes. Carbon 44:2498–2507. doi:10.1016/j.carbon.2006.05.022
30. Rufford TE, Hulicova-Jurcakova D, Zhu Z, Lu GQ (2009) Empirical analysis of the contributions of mesopores and micropores to the double-layer capacitance of carbons. J Phys Chem C 113:19335–19343. doi:10.1021/jp905975q
31. Frackowiak E (2007) Carbon materials for supercapacitor application. Phys Chem Chem Phys 9:1774–1785. doi:10.1039/b618139m
32. Frackowiak E, Béguin F (2002) Electrochemical storage of energy in carbon nanotubes and nanostructured carbons. Carbon 40:1775–1787. doi:10.1016/S0008-6223(02)00045-3
33. Portet C, Yushin G, Gogotsi Y (2007) Electrochemical performance of carbon onions, nanodiamonds, carbon black and multiwalled nanotubes in electrical double layer capacitors. Carbon 45:2511–2518. doi:10.1016/j.carbon.2007.08.024
34. Qu D, Shi H (1998) Studies of activated carbons used in double-layer capacitors. J Power Sources 74:99–107. doi:10.1016/s0378-7753(98)00038-x